SNOW COVER MAPPING AND ICE AVALANCHE MONITORING FROM THE SATELLITE DATA OF THE SENTINELS

Shixin Wang [1], Baolin Yang [1, 2], Yi Zhou [1, *], Futao Wang [1, *], Rui Zhang [1, 2] and Qing Zhao [1]

[1.]Chinese Academy of Sciences, Institute of Remote Sensing and Digital Earth, Beijing 100101, China – (wangsx, yangbl, zhouyi, wangft)@radi.ac.cn; ruizh0921@163.com; qingzhao70@tom.com

[2.]University of Chinese Academy of Sciences, Beijing 100049, China

Commission III, ICWG III/IVa

KEY WORDS: Snow Cover, Ice Avalanche, Sentinels

ABSTRACT:

In order to monitor ice avalanches efficiently under disaster emergency conditions, a snow cover mapping method based on the satellite data of the Sentinels is proposed, in which the coherence and backscattering coefficient image of Synthetic Aperture Radar (SAR) data (Sentinel-1) is combined with the atmospheric correction result of multispectral data (Sentinel-2). The coherence image of the Sentinel-1 data could be segmented by a certain threshold to map snow cover, with the water bodies extracted from the backscattering coefficient image and removed from the coherence segment result. A snow confidence map from Sentinel-2 was used to map the snow cover, in which the confidence values of the snow cover were relatively high. The method can make full use of the acquired SAR image and multispectral image under emergency conditions, and the application potential of Sentinel data in the field of snow cover mapping is exploited. The monitoring frequency can be ensured because the areas obscured by thick clouds are remedied in the monitoring results. The Kappa coefficient of the monitoring results is 0.946, and the data processing time is less than 2 h, which meet the requirements of disaster emergency monitoring.

1. INTRODUCTION

Snow cover mapping plays a very important role in the rapid and accurate assessment of the extent and degree of a snow disaster, such as an ice avalanche. Snow cover can be mapped from remote sensing data at a large scale and with high precision (Immerzeel et al., 2009). Snow cover mapping methods based on multispectral remote sensing have been developed for a long time (Fily et al., 1997; Painter et al., 2009). Based on the high reflectance of snow in some wavelengths compared with other natural targets, optical and near-infrared sensors can distinguish between snow-covered and snow-free ground (Warren, 1982). Landsat-7 ETM+ data were used for mapping snow and ice automatically (Sirguey et al., 2009; Taccardi, 2012), and an estimated error was given (Paul et al., 2013). The fractional snow cover can be provided by a method based on the Normalized Difference Snow Index (NDSI) of Moderate-resolution Imaging Spectrometer (MODIS) (Salomonson and Appel, 2004; Fraser et al., 2010). Sub-pixel snow cover mapping using spectral unmixing was studied, particularly for alpine snow (Painter et al., 1998; Painter et al., 2003).

* Corresponding author

However, accompanied by a large number of obscured areas due to clouds, multispectral remote sensing is often affected by harsh weather in snow-covered areas (Grenfell et al., 1994). Because microwaves have the characteristics of penetrating clouds, in the process of disaster emergency monitoring, microwave imaging is an effective data source. As an active microwave remote sensing technology, Synthetic Aperture Radar (SAR) is often used in snow cover mapping. Passive microwave remote sensing technology is also used in snow cover information extraction; however, the resolution of passive microwave remote sensing is low (Robinson et al., 1984).

Using change detection methods, some repeat-pass spaceborne SAR systems are useful in regular snow cover monitoring, such as the ERS-1/2, JERS-1, and RADARSAT-1/2 (Koskinen et al., 1999; Nagler and Rott, 2000). In addition, SIR-C (Shi et al., 1997), ASAR (Kumar and Venkataraman, 2011) and other SAR data were commonly used in snow cover mapping. The Sentinel-1 Single Look Complex (SLC) wide-swath product was used to retrieve glacier surface velocities (Sánchez-Gámez and Navarro, 2017). Polarimetric SAR (PolSAR) offers additional parameters to discriminate between snow and bare ice areas (Floricioiu and Rott, 2001). Multispectral remote sensing data (Landsat-7) and SAR data (RADARSAT-1) were combined to create an image mosaic set in the Greenland Ice Mapping Project (GIMP) (Howat et al., 2014).

For snow cover mapping, using the coherence of the repeat-pass Interferometric SAR (InSAR) data is a very effective method. An InSAR coherence image is a cross-correlation product derived from two coregistered complex-valued SAR images. A loss of InSAR coherence is often referred to as decorrelation. InSAR has been widely applied to measure glacier topography and displacements (Joughin et al., 1998). Snow cover has considerable impacts on InSAR coherence values; specifically, the coherence values of snow-covered grounds are lower than those of snow-free grounds, based on which a threshold slicing algorithm (TSA) has been developed for snow cover mapping (Kumar and Venkataraman, 2011). The measurement of InSAR coherence between two repeat passes of C-band SAR offers a way to acquire shallow dry snow areas (Zebker and Villasenor, 1992). The research results show that the coherence of the snow cover is approximately 0.31 and the coherence of a thick snow layer is lower (Kumar and Venkataraman, 2011). Lakes and forests also cause decorrelation; however, the snow cover can be distinguished from them (Shi et al., 1997; Strozzi et al., 1999). Compared with the real snow cover results, the accuracy of the snow cover mapping based on InSAR data coherence can reach more than 80%.

2. STUDY AREA

On July 17, 2016, an ice avalanche, the volume of which was approximately 60-70 million cubic meters, occurred in the western Aru Co lake, Rutog county, Ngari prefecture, western Tibet, killing 9 herders and hundreds of animals. The center of this ice avalanche was located at 82°23'21"E, 34°0'3"N. On September 21, 2016, another ice avalanche occurred southeast of the first avalanche. A sketch map of the delineated study area for these ice avalanches is shown in Figure 1.

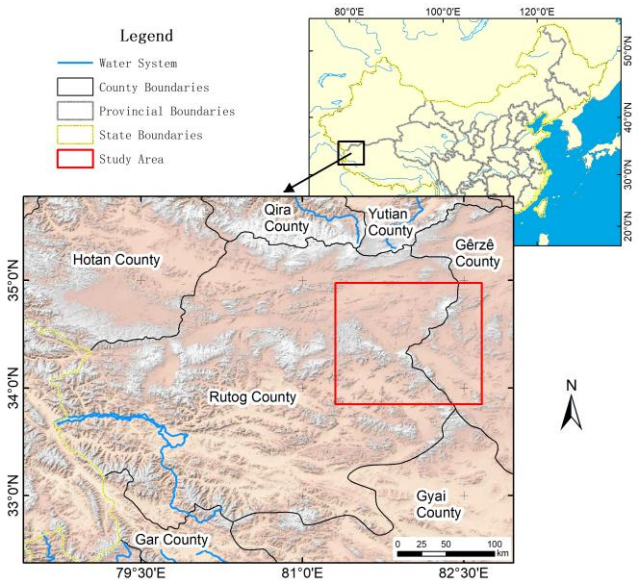

Figure 1. Sketch map of the study area in Rutog county, Ngari prefecture

3. MATERIALS AND METHODS

3.1 Sentinel-1 Satellite Data

The Sentinels are a fleet of European Space Agency (ESA) satellites designed specifically to deliver data and imagery that are central to the European Copernicus program. Sentinel images can be acquired from the Copernicus Open Access Hub (https://scihub.copernicus.eu/dhus/#/home).

The first Sentinel satellite in the European Copernicus program, Sentinel-1, carries a C-band SAR instrument to provide an all-weather, day-and-night supply of Earth’s surface imagery (Malenovský et al., 2012). The Sentinel-1 mission benefits numerous services that relate to the monitoring of sea ice, the surveillance of marine environments, and the measurement of land surfaces for motion risks and for the management of soils (Berger et al., 2012).

Five phases of predisaster and postdisaster images were acquired for the study area, which were used for the snow cover mapping experiment based on the threshold segmentation of InSAR coherence images. The data list is shown in Table 1.

3.2 Sentinel-2 Satellite Data

The Sentinel-2 satellite is the first multispectral Earth observation satellite in the European Copernicus program (Malenovský et al., 2012). Sentinel-2 carries a wide swath high-resolution multispectral imager with 13 spectral bands. The span of the 13 spectral bands, from the visible and the near-infrared to the shortwave infrared, are at different spatial resolutions from 10 to 60 meters. The combination of the wide swath of 290 km and the frequent revisit times of Sentinel-2 provides continuous views of Earth.

Three phases of predisaster and postdisaster images were acquired by Sentinel-2 for the study area, which were used for the snow cover mapping experiment based on the NDSI method, as well as the visual interpretation process. The data list is shown in Table 2.

No.	Center Point	Acquisition Time	Period	Data Type
1	81°59' 19" E, 34°24' 33" N	June 7, 2016	Before the 1st ice avalanche	VV polarized, IW mode, SLC images
2	81°59' 18" E, 34°24' 37" N	July 1, 2016		
3	81°54' 36" E, 34°38' 12" N	August 7, 2016	After the 1st ice avalanche	
4	81°54' 42" E, 34°38' 12" N	August 31, 2016		
5	81°53' 6" E, 34°29' 55" N	September 24, 2016	After the 2nd ice avalanche	

Table 1. Data distribution of Sentinel-1

No.	Center Point	Acquisition Time	Period	Data Type
1	81°0' 10" E, 33°48' 9" N	May 22, 2016	Before the 1st ice avalanche	MSI, L1C images
2	81°0' 10" E, 33°48' 9" N	July 21, 2016	After the 1st ice avalanche	
3	82°45' 54" E, 33°47' 123" N	October 16, 2016	After the 2nd ice avalanche	

Table 2. Data distribution of Sentinel-2

4. METHODS

4.1 Snow Cover Mapping from Sentinel-1

Geocoding and radiation calibration are required to shift the Sentinel-1 raw data from the slanted coordinate system to the geographic coordinate system and to obtain backscattering coefficients. SARscape 5.2 (the manufacturer is Sarmap SA, Cascine di Barico 10, 6989 Purasca, Switzerland) was used in this experiment. It is based on ENVI 5.3 software (the manufacturer is Exelis Visual Information Solutions, Inc., 385 Interlocken Crescent, Suite 300, Broomfield, CO 80021, United States of America). The backscattering coefficient image is shown in Figure 2 (a). It can be seen that the low values appear in both the water bodies and snow cover. However, backscattering coefficients of the newly formed ice avalanche are relatively high (as shown in the yellow frame). Due to the radar penetration into shallow snow, the snow cover with low backscattering coefficients is concentrated at the top of the mountain with thick snow layers. This phenomenon is conducive to divide and differentiate the water bodies and snow

cover. Because that backscattering coefficients and elevations of the water bodies are both relatively low, the water bodies can be extracted using thresholds of the backscattering coefficients and elevations.

The snow cover is mapped by using the decorrelation phenomenon in the InSAR data process. Decorrelation is expressed as the low numerical value in the coherence image. The ice avalanches in the study area occurred in the local snowmelt period; therefore, the causes of decorrelation in this experiment include the changes between the snow cover before and after the ice avalanche and the melting process of the snow. According to these points, the coherence image of Sentinel-1 InSAR data can be segmented by a certain threshold to map the snow cover. The coherence image is shown in Figure 2 (b). It can be seen that the snow cover has low coherence values. However, because of the absorption characteristics of water to electromagnetic waves, low coherence values are also exhibited in the water bodies. Therefore, the water bodies extracted from the backscattering coefficient image must be removed from the coherence segment result. The coherence of the newly formed ice avalanche is low (as shown in the yellow frame), which is beneficial to the extraction of the ice avalanche body.

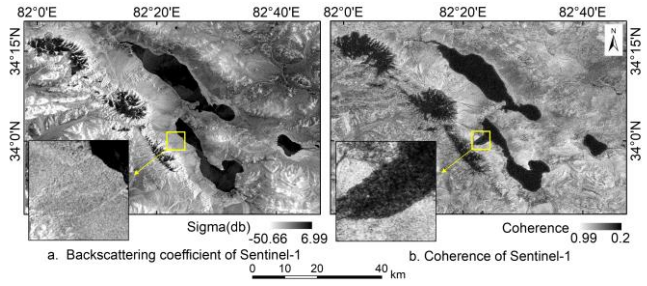

Figure 2. Backscattering coefficient and coherence images from Sentinel-1

4.2 Snow Cover Mapping from Sentinel-2

There are strong reflection characteristics of the snow in the visible light bands and strong absorption characteristics in the shortwave infrared bands. Therefore, the snow cover can be distinguished by using the visible light bands and shortwave infrared bands.

The Sen2Cor software (Sentinel-2 atmospheric Correction, also known as Sentinel-2 Level-2A Prototype Processor; the manufacturer is the European Space Agency, Largo Galileo Galilei 1, Casella Postale 64, I-00044 Frascati, Italy) is used to conduct atmospheric correction to the Sentinel-2 images. It is provided by the European Space Agency (ESA) (Main-Knorn et al., 2015). Its purpose is to process the Level-1C (L1C) Top of Atmosphere (TOA) image data into a Level-2A Bottom of Atmosphere (BOA) reflectance product. The core of the algorithm is an atmospheric radiative transfer model, Library for Radiative transfer calculation (LibRadtran) (Mayer and Kylling, 2005).

After the atmospheric correction, a snow confidence map is produced from NDSI (Salomonson and Appel, 2004). The Sentinel-2 natural-color image and the snow confidence map are shown in Figure 3. It can be seen that the confidence values are relatively high for the snow cover that is not obscured by thick clouds. However, because of the impact of thick clouds, the boundaries of the snow are not complete (as shown in the yellow frame).

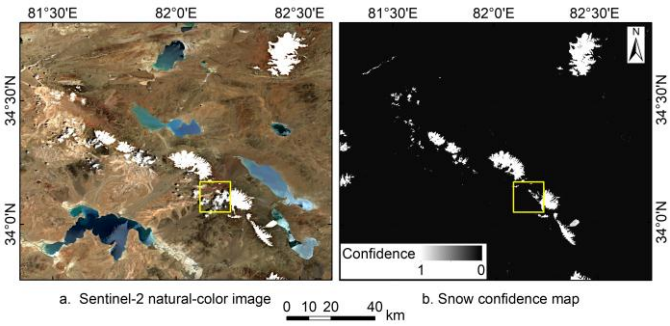

Figure 3. Natural-color image and the snow confidence map of Sentinel-2

4.3 Technical Process of Snow Cover Mapping

Through the above analyses, it is feasible to remedy the thick cloud areas in the snow cover mapping result from Sentinel-2 with the snow cover mapping result from the Sentinel-1. By merging the snow cover results from Sentinel-1 and Sentinel-2, the final snow cover map can be obtained. The flow chart of the snow cover mapping process based on the satellite data of the Sentinels is shown in Figure 4.

.

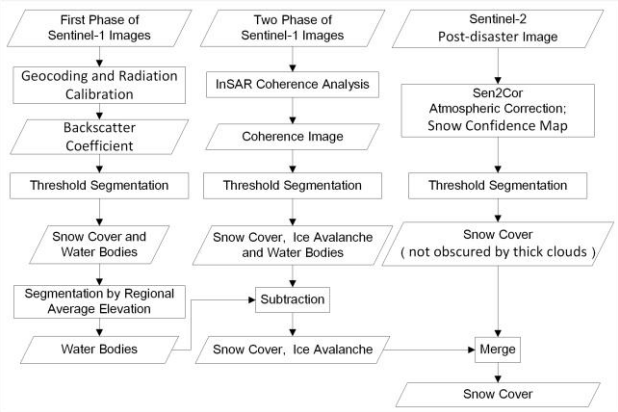

Figure 4. Flow chart of the snow cover mapping process

5. RESULTS

5.1 Snow Cover Mapping from the Sentinels

Based on the statistical analysis of the snow confidence map with the visual interpretation result of the snow cover in the areas without clouds as a reference, the threshold of the snow confidence map was set to 0.8 to map the snow cover. The snow cover mapping result from Sentinel-2 is shown in Figure 5(a).

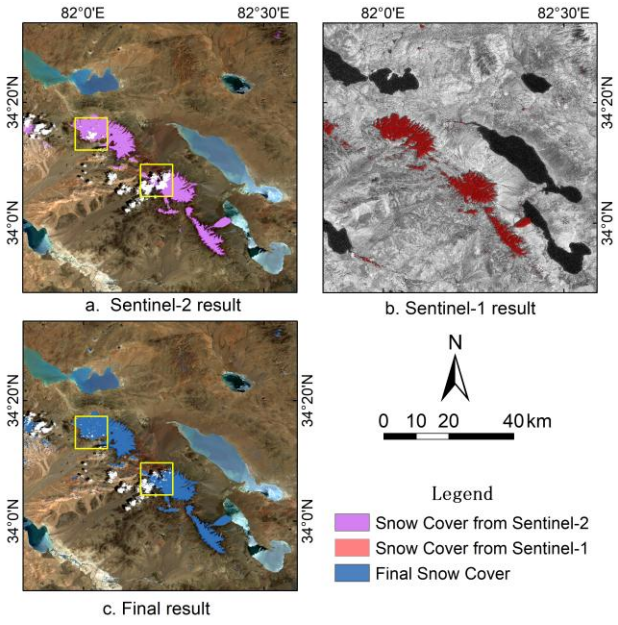

Figure 5. Snow cover mapping results from the Sentinels

Based on the statistical analysis of the backscattering coefficients and coherence values with the visual interpretation result of the snow cover in the areas without clouds as a reference, the backscattering coefficient threshold was set to -15 db, and the coherence threshold was set to 0.43 to map the snow cover. The regional average elevation, which was calculated from the New Global Digital Elevation Model (GDEM V2), was used as the elevation threshold. The snow cover mapping results from Sentinel-1 is shown in Figure 5(b).

The snow cover maps were obtained from the comprehensive utilization of Sentinel-1 and Sentinel-2 data. The final snow cover mapping result is shown in Figure 5(c). It can be seen from the yellow frame that the incomplete mapping of the snow cover caused by the thick cloud obscuration has been remedied.

5.2 Ice Avalanche Monitoring

The snow cover mapping results from the predisaster data, the first ice avalanche data and the second ice avalanche data were obtained to monitor the ice avalanches, as shown in Figure 6. It clearly shows the influence extents of the two ice avalanches. From the yellow frame in Figure 6, it can be seen that the foot of the first ice avalanche, which had slid into the lake, melted before the second ice avalanche.

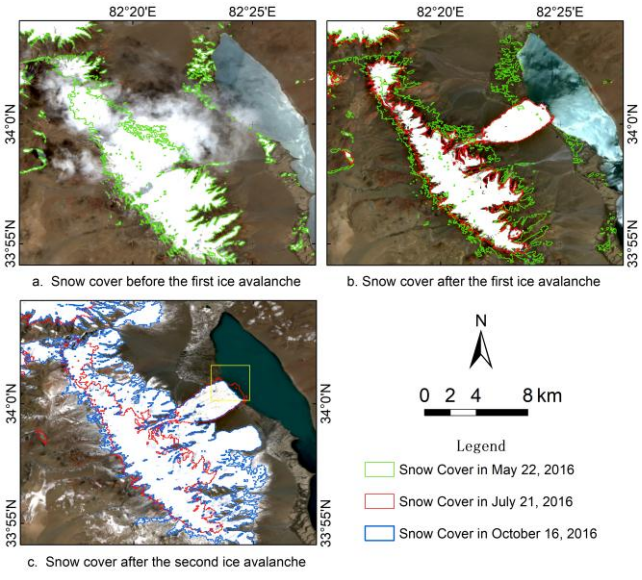

Figure 6. Snow cover changes during the ice avalanches

Based on the snow cover mapping, the snow cover changes were counted for on the mountain where the ice avalanches were located. The statistical results are shown in Table 3. The processing of the snow cover maps could be completed in 2 h

using Intel Core i7-3770 CPU and 16 G memory, which met the requirements of ice avalanche emergency monitoring.

	Snow Cover Area (ha)	Area Change (ha)
Before the 1st Ice Avalanche	5940.85	-935.74
After the 1st Ice Avalanche	5005.11	18564.66
After the 2nd Ice Avalanche	23569.77	

Table 3. Snow cover area statistics for the mountain where the ice avalanches were located

6. DISCUSSION

The accuracy of the snow cover mapping was further evaluated by the Kappa coefficient. The Kappa coefficient is shown in Equation (1):

$$\text{Kappa} = \frac{(a+b+c+d)(a+d)-(a+c)(a+b)-(\text{d+c})(\text{d+b})}{(a+b+c+d)^2-(a+c)(a+b)-(d+c)(\text{d+b})} \quad (1)$$

where a, b, c, d = the number of true positives, false positives, true negatives and false negatives in the confused matrix.

The accuracy evaluation is shown in Table 4. The snow cover mapping accuracy of this method was relatively high; thus, this method met the application requirements for ice avalanche emergency monitoring.

		Visual Interpretation Results (ha)	
		Snow Cover	No snow Cover
Snow Cover Mapping Results (ha)	Snow Cover	60024.31	2978.98
	No snow Cover	3573.16	1427614.42
Kappa Coefficient = 94.60%			

Table 4. Accuracy of the snow cover mapping result

The accuracy of the proposed method is similar to or better than that of most of the other methods using remote sensing images with medium resolution, except that of the subpixel snow cover mapping algorithm using an airborne hyperspectral image (as good as 95%) (Jebur et al., 2014; Chen et al., 2014). However, mapping snow cover with satellite images from the Sentinels has the advantage of wide monitoring coverage. Moreover, the process of information extraction for ice avalanches is synchronized with the temporal order of the satellite image acquisition and makes full use of the acquired multispectral images and SAR images when the data are not complete under emergency conditions. The timely completion and the adequate frequency of the monitoring results can be ensured.

The optical properties and microwave properties of the snow cover are applied in the proposed method. The snow cover mapping method based on spectral features can be applied to other multispectral satellite data that have shortwave infrared bands, such as Landsat-8 and MODIS. The snow cover mapping method based on the threshold segmentation of InSAR coherence images can be applied to other SAR satellite data, such as Radarsat-1/2 and TanDEM-X, which can acquire interference image pairs.

The snow cover and ice avalanche map was also obtained by the removal of the known water bodies from the threshold segmentation result of the Sentinel-1 coherence image. The extracted snow cover and ice avalanches are shown in Figure 7.

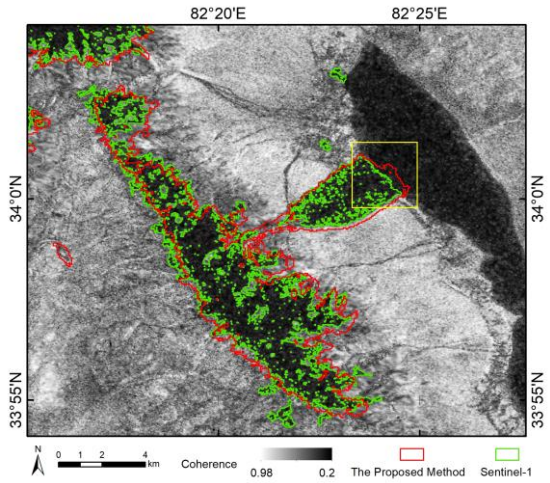

Figure 7. Comparison of the snow cover mapping result of the proposed method and that of Sentinel-1 after removal of the known water bodies

It can be seen that the result of the Sentinel-1 after the removal of water bodies cannot effectively display the foot of the ice avalanche that slid into the lake. Therefore, it cannot reflect the phenomenon of ice melting in the lake, as shown in Figure 6 of Section 5.2.

7. CONCLUSIONS

Snow cover mapping results were generated from the InSAR coherence image of Sentinel-1 and the atmospheric correction result of Sentinel-2 for the study area in Rutog county, Ngari prefecture, western Tibet. The comparison of the extracted snow cover and the visual interpreted snow cover showed that the accuracy of the mapping result was equivalent to that of the visual interpretation result. The applicability of the method and the accuracy of the results were analyzed and evaluated. The extraction accuracy and time consumption met the application requirements for ice avalanche emergency monitoring.

The innovations of this paper were as follows. First, an appropriate method of snow cover mapping from images of the Sentinel satellites was proposed, and the application potential of the Sentinel data in the field of snow cover mapping was exploited. Second, the snow cover mapping method based on the microwave features of SAR images and that based on the spectral features of multispectral images have been applied in collaboration, which not only avoids the interference of thick cloud obscuration on the mapping results but also ensures the accuracy of the mapped boundary.

ACKNOWLEDGEMENTS

This research was funded by the National Key Research and Development Program of China (2017YFB0504101, 2016YFC0803004), the Special Project on High Resolution of Earth Observation System (No. 00-Y30B15-9001-14/16) and the Youth Innovation Promotion Association of the CAS (2015129).

REFERENCES

Berger, M.,Moreno, J.,Johannessen, J.A.,Levelt, P.F. and Hanssen, R.F., 2012. ESA's sentinel missions in support of earth system science. *Remote Sensing of Environment*, 120, pp. 84-90.

Chen, F.,Lin, H. and Hu, X., 2014. Slope superficial displacement monitoring by small baseline SAR interferometry using data from l-band ALOS PALSAR and x-band TerraSAR: A case study of hong kong, china. *Remote Sensing*, 6(2), pp. 1564-1586.

Fily, M.,Bourdelles, B.,Dedieu, J.P. and Sergent, C., 1997. Comparison of in situ and Landsat Thematic Mapper derived snow grain characteristics in the alps. *Remote Sensing of Environment*, 59(3), pp. 452-460.

Floricioiu, D. and Rott, H., 2001. Seasonal and short-term variability of multifrequency, polarimetric radar backscatter of Alpine terrain from SIR-C/X-SAR and AIRSAR data. *IEEE Transactions on Geoscience & Remote Sensing*, 39(12), pp. 2634-2648.

Fraser, A.D.,Massom, R.A. and Michael, K.J., 2010. Generation of high-resolution East Antarctic landfast sea-ice maps from cloud-free MODIS satellite composite imagery. *Remote Sensing of Environment*, 114(12), pp. 2888-2896.

Grenfell, T.C.,Warren, S.G. and Mullen, P.C., 1994. *Reflection of solar radiation by the Antarctic snow surface at ultraviolet, visible, and near-infrared wavelengths*, pp. 18669-18684.

Howat, I.M.,Negrete, A. and Smith, B.E., 2014. The Greenland Ice Mapping Project (GIMP) land classification and surface elevation data sets. *The Cryosphere*, 8(4), pp. 1509-1518.

Immerzeel, W.W.,Droogers, P.,Jong, S.M.D. and Bierkens, M.F.P., 2009. Large-scale monitoring of snow cover and runoff simulation in Himalayan river basins using remote sensing. *Remote Sensing of Environment*, 113(1), pp. 40-49.

Jebur, M.N.,Pradhan, B. and Tehrany, M.S., 2014. Detection of vertical slope movement in highly vegetated tropical area of Gunung pass landslide, Malaysia, using L-band InSAR technique. *Geosciences Journal*, 18(1), pp. 61-68.

Joughin, I.R.,Kwok, R. and Fahnestock, M.A., 1998. Interferometric estimation of three-dimensional ice-flow using ascending and descending passes. *IEEE Transactions on Geoscience & Remote Sensing*, 36(1), pp. 25-37.

Koskinen, J.,Metsämäki, S.,Grandell, J.,Jänne, S.,Matikainen, L. and Hallikainen, M., 1999. Snow monitoring using radar and optical satellite data. *Remote Sensing of Environment*, 69(1), pp. 16-29.

Kumar, V. and Venkataraman, G., 2011. SAR interferometric coherence analysis for snow cover mapping in the western Himalayan region. *International Journal of Digital Earth*, 4(1), pp. 78-90.

Main-Knorn, M.,Pflug, B. and Debaecker, V., 2015. Calibration and Validation plan for the L2A processor and products of the Sentinel-2 mission. In: *The International Archives of the Photogrammetry, Remote Sensing and Spatial Information Sciences*, Berlin, Germany, Vol. XL-7/W3, pp. 1249-1255.

Malenovský, Z.,Rott, H.,Cihlar, J.,Schaepman, M.E.,García-Santos, G.,Fernandes, R. and Berger, M., 2012. Sentinels for science: Potential of Sentinel-1, -2, and -3 missions for scientific observations of ocean, cryosphere, and land. *Remote Sensing of Environment*, 120(10), pp. 91-101.

Mayer, B. and Kylling, A., 2005. Technical note: The libRadtran software package for radiative transfer calculations - description and examples of use. *Atmospheric Chemistry & Physics*, 5(2005), pp. 1855-1877.

Nagler, T. and Rott, H., 2000. Retrieval of wet snow by means of multitemporal SAR data. *IEEE Transactions on Geoscience & Remote Sensing*, 38(2), pp. 754-765.

Painter, T.H.,Dozier, J.,Roberts, D.A.,Davis, R.E. and Green, R.O., 2003. Retrieval of subpixel snow-covered area and grain size from imaging spectrometer data. *Remote Sensing of Environment*, 85(1), pp. 64-77.

Painter, T.H.,Rittger, K.,Mckenzie, C.,Slaughter, P.,Davis, R.E. and Dozier, J., 2009. Retrieval of subpixel snow covered area, grain size, and albedo from MODIS. *Remote Sensing of Environment*, 113(4), pp. 868-879.

Painter, T.H.,Roberts, D.A.,Green, R.O. and Dozier, J., 1998. The Effect of Grain Size on Spectral Mixture Analysis of Snow-Covered Area from AVIRIS Data. *Remote Sensing of Environment*, 65(3), pp. 320-332.

Paul, F.,Barrand, N.E.,Baumann, S.,Berthier, E.,Bolch, T.,Casey, K.,Frey, H.,Joshi, S.P.,Konovalov, V. and Bris, R.L., 2013. On the accuracy of glacier outlines derived from remote-sensing data. *Annals of Glaciology*, 54(63), pp. 171-182.

Robinson, D.,Kunzi, K.,Kukla, G. and Rott, H., 1984. Comparative utility of microwave and shortwave satellite data for all-weather charting of snow cover. *Nature*, 312(5993), pp. 434-435.

Salomonson, V.V. and Appel, I., 2004. Estimating fractional snow cover from MODIS using the normalized difference snow index. *Remote Sensing of Environment*, 89(3), pp. 351-360.

Sánchez-Gámez, P. and Navarro, F., 2017. Glacier surface velocity retrieval using D-InSAR and offset tracking techniques applied to ascending and descending passes of Sentinel-1 data for southern Ellesmere ice caps, Canadian Arctic. *Remote Sensing*, 9(5), pp. 442.

Shi, J.,Hensley, S. and Dozier, J., 1997. Mapping snow cover with repeat pass synthetic aperture radar. In: *Geoscience and Remote Sensing, 1997. IGARSS '97. Remote Sensing - A Scientific Vision for Sustainable Development., 1997 IEEE International*, Vol.2, pp. 628-630.

Sirguey, P.,Mathieu, R.,Arnaud, Y. and Khan, M.M., 2009. Improved resolution for the detection of snow with MODIS using wavelet fusion. In: *Geoscience and Remote Sensing Symposium, 2007. IGARSS 2007. IEEE International*, 3975-3978.

Strozzi, T.,Wegmuller, U. and Matzler, C., 1999. Mapping wet snowcovers with SAR interferometry. *International Journal of Remote Sensing*, 20(12), pp. 2395-2403.

Taccardi, B., 2012. The first complete inventory of the local glaciers and ice caps on Greenland. *Cryosphere*, 6(6), pp. 1483-1495.

Warren, S.G., 1982. Optical properties of snow. *Reviews of Geophysics*, 20(1), pp. 67-89.

Zebker, H.A. and Villasenor, J., 1992. Decorrelation in interferometric radar echoes. *IEEE Transactions on Geoscience & Remote Sensing*, 30(5), pp. 950-959.